Crystallization and the liquid-liquid critical point in nonbonded modified-WAC models

E. Lascaris,[1] Francesca Marchese,[1] and Nicole Gaspar[1]
Department of Chemistry & Physical Sciences, Pace University, New York, NY 10038 USA

(*Electronic mail: elascaris@pace.edu)

(Dated: 25 June 2024)

For decades, it has been known that Liquid-Liquid Critical Points (LLCPs) can exist in one-component liquids, yet a comprehensive understanding of the conditions under which they arise remains elusive. To better comprehend the possible interplay between the LLCP and the crystalline phase, we conduct molecular dynamics simulations using the nonbonded family of modified-WAC (mWAC) models, which are known to exhibit a LLCP for certain parameter values. By comparing different versions of the mWAC model—those featuring a LLCP and those lacking one—we identify several key differences between the models relating to crystallization. Those models which do have a LLCP are found to have multiple stable crystalline phases, one of them being a solid-state ionic conductor similar to superionic ice. Moreover, we find that for models that do not have a LLCP, the liquid becomes a glass at a larger range of temperatures, possibly preventing the occurrence of a LLCP. Further studies are required to determine if these results are general or model-specific.

I. INTRODUCTION

When mixing oil and water, the two liquids separate into two distinct layers. This type of two-component phase separation is well-known and well-understood. However, that such a phenomenon may also occur in a *one-component* system (e.g., liquid water only) is far from obvious[1], and has not been given much consideration until the discovery by Poole et al.[2] in 1992 of a possible liquid-liquid critical point in computer simulations of the ST2 model of water[3]. According to the so-called liquid-liquid critical point hypothesis of water, at high pressures and low temperatures (below the melting line), pure liquid water exists in two different states: a low-density liquid (LDL) and a high-density liquid (HDL). These two liquid phases undergo a phase separation at the liquid-liquid phase transition (LLPT) line, which ends at a liquid-liquid critical point (LLCP) that is located deep in the supercooled regime of the phase diagram, a region that is extremely hard to reach in experiments[2,4–8].

If real experimental water has a LLCP remains a matter of debate[9–17], but that a liquid-liquid phase separation can occur in a one-component system has been unequivocally demonstrated in a variety of liquids. For instance, after simulations done by Hohl and Jones[18] predicted a possible LLPT in liquid phosphorus (P), Katayama et al. were able to confirm this experimentally in 2000 using in situ X-ray diffraction[19–21]. They were able to directly observe the coexistence of two forms of liquid P, a polymeric network-forming liquid and a molecular liquid of P_4 molecules[22,23]. Similarly, a LLPT has been predicted to exist in liquid silicon (Si), first by Aptecar[24] in 1979, then by Sastry and coworkers in 2003 using molecular dynamics simulations[25,26], and later by first-principle simulations[27,28]. In 2010, Beye et al. experimentally confirmed the existence of a LLPT in silicon by monitoring its electronic structure while heating the silicon into different phases using ultrashort optical laser pulses[29].

LLPTs have been predicted and/or observed in several other liquids, including sulfur (S)[30,31], carbon (C)[32,33], silica (SiO_2)[34–37], and organic molecular liquids such as triphenyl phosphate (TPP)[38–45]. Unfortunately, the existence of a LLPT in these liquids remains controversial[46–55], as it is hard to witness the transition experimentally. The transition line typically lies deep within the supercooled region of the phase diagram, where the liquid crystallizes long before the transition between two meta-stable liquids can be observed[31]. Nonetheless, simulations have indicated that the LLPT does not necessarily occur only between two meta-stable liquids; it is possible to have this occur between two stable liquids as well[56].

Although a significant amount of research has been done, it remains unclear under exactly what circumstances a one-component liquid would have a LLPT. To study this interesting phenomenon to a better degree, a model was developed by Lascaris in 2016 called the *modified-WAC model*[57–60]. Based on the WAC model for liquid silica (SiO_2)[61], the modified-WAC (mWAC) model consists of a 1:2 mixture of positive Si ions and negative O ions that interact via electrostatics as well as ion-dependent interaction potential. A unique property of the mWAC model is that a small adjustment of the ion charges by a factor of f_q can either introduce or eliminate the LLCP, thus making it an excellent model to study in-depth the conditions under which a LLPT or LLCP appears. Note that this mixture of Si and O ions is still a one-component liquid, as the positive Si and negative O ions do not phase separate, but instead form two different liquid SiO_2 structures. Furthermore, a bonded version of this model[60] demonstrates that the LLPT can also appear when the ions are bound together in a SiO_2 molecule through intramolecular bonds similar to those between the H and O atoms forming an H_2O molecule.

One feature that many liquids with a LLPT seem to have is polymorphism; the existence of multiple stable crystal structures. Phosphorus (P), for example, has many allotropes in the solid state[19,62,63] such as white P consisting of tetrahedral P_4 molecules, black P having a layered structure, and red P typically being amorphous. Silicon (Si) only forms a diamond cubic crystal at standard pressure, but upon increasing the pressure many other crystal structures can be observed[64–69].

If the molecules of a substance can form multiple crystal structures, it might be possible to have multiple liquid structures as well, a phenomenon called "liquid polymorphism" or "polyamorphism"[70]. A possible connection between having multiple crystal structures and multiple liquid structures invites us to study the crystalline phase in more detail using the modified-WAC model.

In the present work, we study the crystalline state of the nonbonded modified-WAC model of Ref. 57, and determine how the crystal phase is affected when we change f_q, the parameter that introduces or eliminates the LLCP in this model. In addition to considering the crystal structure of mWAC, we also consider the location of the melting line since it remains an open question under which circumstances the liquid-liquid transition is between two stable liquids vs. two meta-stable liquids. If the LLCP occurs below the melting line, we obtain a situation like that predicted for liquid water, with phase separation between two meta-stable liquids (meta-stable with respect to the crystal). Alternatively, if the LLCP lies above the melting line, then the critical point is easily accessible and does not compete with the effects of crystallization.

The melting temperature, at a given pressure, is the temperature at which a liquid and a crystal are together in a stable equilibrium, neither state being the preferred one. As is well-known, it is possible to cool a liquid to a temperature below the melting temperature, thus creating a meta-stable supercooled liquid. Upon lowering the temperature further, preventing crystallization becomes more and more difficult. The lowest temperature a liquid can attain depends on how the liquid is studied. In theory, the lowest temperature is at the spinodal, where both the isothermal compressibility K_T and the isobaric heat capacity C_P simultaneously become infinite[71]. Beyond this limit the liquid becomes unstable and immediately crystallizes. It is impossible to actually reach the spinodal line with experiments; the liquid will instead crystallize spontaneously at the homogeneous nucleation line, a limit that depends on how the experiment is executed as well as the speed at which measurements are done. In computer simulations it is difficult to reach the spinodal as well, although the homogeneous nucleation line will typically lie closer to the spinodal because methods such as molecular dynamics study the liquid at picosecond and nanosecond time scales.

Similarly to supercooling a liquid, one can also superheat a crystal[72–74]. The mechanisms involved are very similar; one can heat the meta-stable crystal above the melting temperature, until the crystal spinodal is reached above which the crystal becomes unstable and will immediately melt. In this work we shall measure the melting line as well as estimate both the liquid and the crystal spinodal lines.

II. METHODS

The modified-WAC (mWAC) model is a modified version of the original WAC model introduced by Woodcock, Angell, and Cheeseman[61] to simulate liquid silica (SiO_2). In the original model the liquid consists of a 1:2 mixture of Si^{4+} and O^{2-} ions that do not have any explicit bonds and only interact via electrostatics and a repulsive force that represents the interpenetration of electron shells[75]. The nonbonded mWAC model we consider here uses the same interaction potential, except that the ion charges are multiplied by a factor f_q:

$$U(r_{ij}) = \frac{1}{4\pi\varepsilon_0}\frac{(f_q q_i)(f_q q_j)}{r_{ij}^2} + A_{ij}\exp(-B\,r_{ij}) \qquad (1)$$

Here the subscripts $i, j = \{\mathrm{Si}, \mathrm{O}\}$ indicates the ion type. The parameters in the mWAC model are identical to those of the original WAC model[37,76]: $A_{\mathrm{Si,Si}} = 1.917\,991\,469\times10^5$ kJ/mol, $A_{\mathrm{Si,O}} = 1.751\,644\,217\times10^5$ kJ/mol, $A_{\mathrm{O,O}} = 1.023\,823\,519\times10^5$ kJ/mol, and $B = 34.48$ nm^{-1}.

The existence of a LLCP in mWAC is made most evident by drawing the isochores in a *P-T* diagram such as those shown in Fig. 1. Previous studies[57,58] indicate that the nonbonded mWAC model has a clear LLCP when $f_q = 0.84$ (i.e., when $q_{\mathrm{Si}} = +3.36e$ and $q_{\mathrm{O}} = -1.68e$) which vanishes as the parameter is increased to $f_q = 0.96$. When $f_q = 1.08$ there is no longer any sign of a LLCP. When we decrease the value of f_q to below 0.84, the LLCP moves to lower temperatures and pressures. At $f_q = 0.72$ the LLCP disappears below the vapor line, although a liquid-liquid transition region is still accessible.

We simulate the model using Gromacs[77–82]. We are forced to use an old version (4.6.7), since later versions no longer support potentials such as those of Eq. 1. Using an old version of Gromacs has no effect on the quality of the simulations, although it does negatively affect the time needed to complete them. Additionally, compiling the Gromacs 4.6.7 source code requires the application of certain settings, as explained in Ref. 60.

All simulations are done using the constant-pressure, constant-temperature (NPT) ensemble, with $N = 3000$ ions. Simulations of the crystal state are simulated using an anisotropic barostat, which allows for the system to shrink or expand independently in the *x*-, *y*-, and *z*-direction. Simulations of the liquid, however, require the use of an *isotropic* barostat to prevent the simulation box from deforming too much, which can cause Gromacs to crash. Forcing the box to deform in all directions equally prevents this.

To measure the location of the melting line using molecular dynamics, one can simulate an elongated box that is half liquid and half crystal. However, this requires knowledge of the crystal structure, which has not yet been determined for mWAC. Fortunately, previous research has indicated that the original WAC model undergoes spontaneous crystallization at pressures of 40 GPa and above[37], which provides an excellent starting point for our studies. After obtaining and analyzing the crystal obtained from spontaneous crystallization, we can heat it up to see if any additional crystalline states appear.

We run four versions of the mWAC model ($f_q = 0.72, 0.84, 0.96, 1.08$) at high pressures near 40 GPa. We start at a relatively high temperature and then slowly try lower and lower temperatures until we find a temperature at which the system spontaneously crystallizes. During each run we take care to simulate the liquid for at least 3 times the equilibration time (3τ), with the equilibration time τ estimated by the

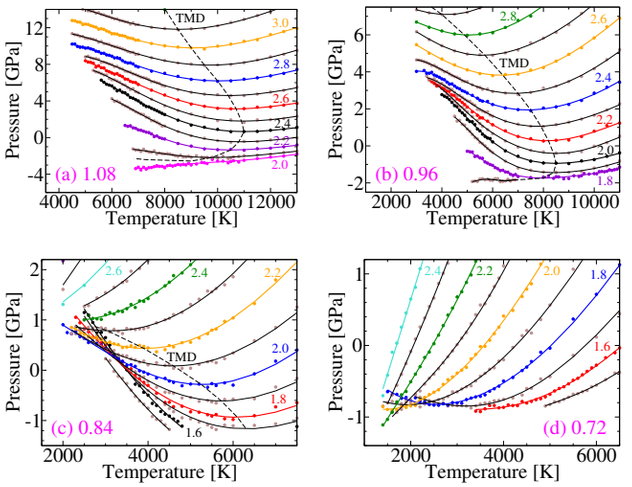

FIG. 1. **Crossing isochores makes the liquid-liquid critical point (LLCP) in mWAC models clearly visible.** Data taken from Ref. 57. Numbers next to isochores indicate density in g/cm^3, TMD indicates Temperature of Maximum Density. (a) No crossing of isochores is observed when $f_q = 1.08$, which means that at each state point (P,T) there is only one liquid phase. (b) As f_q is decreased, we find that the isochores come closer. The liquid becomes too glassy at temperatures below 3000–4000 K, which prevents it from reaching a proper meta-stable equilibrium within reasonable simulation times. However, studies of the response functions suggest that no LLCP exists at lower temperatures for $f_q = 0.96$[37,57]. (c) A region where the isochores are crossing is clearly visible for the nonbonded mWAC model with $f_q = 0.84$. The liquid can exist at two different densities simultaneously at any given state point (P,T) within this region, which suggests a coexistence of two different liquids with different densities. Detailed studies[58] confirm that a LLCP indeed exists at $(\rho_c, T_c, P_c) = (1.8$ g/cm^3, 3350 K, 0.19 GPa). (d) Upon further lowering the value of f_q to 0.72, the LLCP disappears below the liquid-vapor line at low T and low P, although the liquid-liquid coexistence region is still visible.

average time it takes for an O ion to move twice its diameter of 0.28 nm (same convention as used in Ref. 57). The equilibration time τ increases rapidly as we move to lower temperatures, until at some pressure $P_{\mathrm{sc,min}}$ we are no longer able to observe any spontaneous crystallization because it simply takes too long to simulate. In this work we limit our simulations to 200 ns, equivalent to running a simulation for several days in real time.

Once the liquid spontaneously crystallizes, we need to use a method to determine its crystal structure. Visual inspection is hard to do, as the obtained crystal is typically in some random orientation that is not aligned with the sides of the box. Crystalline defects and thermal fluctuations further complicate proper identification. However, various numerical methods for crystal identification have been developed; for example, the common neighbor analysis (CNA)[83], the centrosymmetry parameter analysis (CSP)[84], Voronoi analysis[85], and the neighbor distance analysis technique[85]. It is also possible to consider the radial distribution function (RDF) $g(r)$, which provides a unique "fingerprint" that can be used to identify different crystal lattices—a perfect crystal produces a large set of sharp spikes representing the periodic distances between each atom and its neighbors. Unfortunately, crystalline defects and high temperatures will broaden these spikes significantly, making it difficult to identify the structure correctly. The cumulative RDF (the integral of $g(r)$ over r) is less sensitive to these complications and can be used to measure the average number of nearest neighbors of each atom in the crystal. For instance, each atom has 8 nearest neighbors in the body-centered cubic (bcc) crystal structure, while in face-centered cubic (fcc) crystals and hexagonal close-packed (hcp) crystals each atom has 12 nearest neighbors. Hence, the cumulative RDF can be used to differentiate between these and other crystal structures.

One of the most popular methods is the use of the so-called Steinhardt bond order parameters. Multiple versions of these parameters exist[86–88], but here we shall use the parameters defined by Lechner et al (Ref. 88). These order parameters make use of the spherical harmonics $Y_{\ell m}(\theta,\varphi)$, which are normalized such that $\int |Y_{\ell m}|^2 \sin\theta \,\mathrm{d}\varphi \,\mathrm{d}\theta = 1$. With these we calculate for each atom i,

$$q_{\ell m}(i) = \frac{1}{N_b(i)} \sum_{j=1}^{N_b(i)} Y_{\ell m}(\mathbf{r}_{ij}) \tag{2}$$

where the sum is over all nearest neighbors j of atom i, and $N_b(i)$ is the number of nearest neighbors of atom i. The vector $\mathbf{r}_{ij}$ points from atom i to its neighbor j, which in spherical coordinates provide θ_{ij} and φ_{ij}. The parameters $q_{\ell m}(i)$ can be used to calculate the Steinhardt order parameters:

$$q_\ell(i) = \sqrt{\frac{4\pi}{2\ell+1} \sum_{m=-\ell}^{\ell} |q_{\ell m}|^2} \tag{3}$$

These parameters are sensitive to different symmetries of the crystal, depending on the value of ℓ. Lechner et al. suggest the use of an *averaged* bond order parameter, defined by

$$\bar{q}_\ell(i) = \sqrt{\frac{4\pi}{2\ell+1} \sum_{m=-\ell}^{\ell} |\bar{q}_{\ell m}|^2} \tag{4}$$

where

$$\bar{q}_{\ell m}(i) = \frac{1}{N_b(i)+1} \left(q_{\ell m}(i) + \sum_{j=1}^{N_b(i)} q_{\ell m}(j) \right) \tag{5}$$

In this work we use the averaged bond order parameter $\bar{q}_4$ by Lechner et al., as this parameter distinguishes very nicely between different crystal structures.

Once we have determined the structure of the crystal that was obtained from spontaneous crystallization, we will create a "perfect" version of this crystal to be used for subsequent simulations. A perfect crystal without defects provides a better estimate of the melting line and the crystal spinodal line (the T above which the crystal is unstable), as defects would promote the melting and thus lower the observed melting temperature. Furthermore, we can align the lattice vectors of the

crystal in the x-, y-, and z-direction, which significantly facilitates further analysis. By comparing the radial distribution functions, we can check that our perfect crystal is in fact the same crystal as the one we obtained from spontaneous crystallization.

Finally, we will heat up the perfect crystal to temperatures above its melting temperature, i.e., superheat it. This will allow us to establish the limit of stability of the spontaneous crystal and may also lead to the discovery of additional crystal structures. Any secondary crystal structure can be easily analyzed since its lattice vectors can be expected to remain aligned with the box in a similar way as the original crystal.

III. RESULTS AND DISCUSSION

A. Spontaneous crystallization

For all values of f_q considered here, we find a range of pressures $P \geq P_{\text{sc,min}}$ over which spontaneous crystallization occurs at temperature T_{sc} upon cooling the liquid. We define the homogeneous nucleation line here as the locus of these temperatures, shown in Fig. 2. At temperatures less than T_{sc}, the liquid is no longer meta-stable and becomes unstable with respect to the crystal. Below a pressure of $P_{\text{sc,min}}$ the liquid has become too glassy for us to observe spontaneous crystallization within 200 ns, even though we can still equilibrate the liquid (the equilibration time is about $\tau \sim 50$ ns).

As Fig. 2 demonstrates, we find that spontaneous crystallization happens more easily for lower values of f_q, i.e., those versions of the model for which there is a LLCP present. In fact, for $f_q = 1.08$ we were unable to observe spontaneous crystallization at 40 GPa (as was found in the original WAC model, which corresponds to $f_q = 1.00$); the minimum pressure needed for that version of the model is $P_{\text{sc,min}} = 50$ GPa. Furthermore, it is interesting to note that for $f_q \leq 0.96$ all homogeneous nucleation lines more-or-less overlap, suggesting that a low P_{min} might be strongly correlated with the presence of a LLCP in the model.

B. Identification of crystal structure

The crystal that is formed when the liquid undergoes spontaneous crystallization is found to have a similar structure for all values of f_q. As an example, consider the model with $f_q = 0.84$ which crystallizes spontaneously at $P = 5$ GPa and $T_{\text{sc}} = 2100$ K. In Fig. 3(a) we consider the Si-Si radial distribution function (RDF) $g(r)$ as well as its integral, the cumulative RDF. While the RDF of a perfect crystal consists of numerous discrete spikes, the RDF we obtain for our crystal has these spikes smeared out into a continuous curve because of crystalline defects and thermal fluctuations. Nevertheless, we can use the cumulative RDF to determine the average number of nearest neighbors. The nearest neighbors of an atom are those neighbors that lie within the first peak of the RDF, in this case within a distance of $r = 0.44$ nm, where $g(r)$ has a local minimum. Integrating over $g(r)$ gives us the number

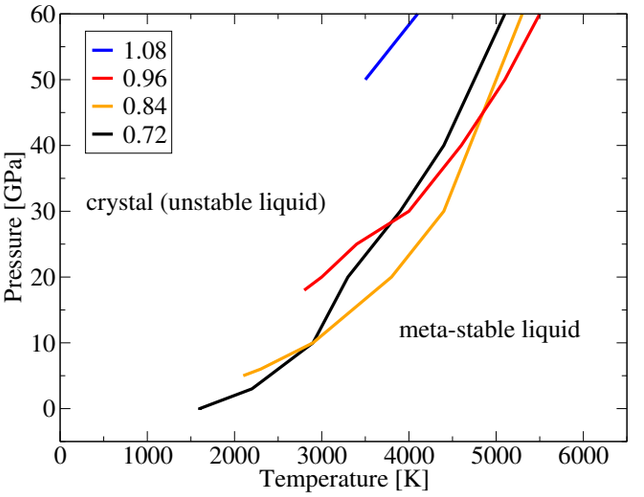

FIG. 2. **Homogeneous nucleation line for different values of f_q.** The mWAC liquid can be supercooled down to a temperature T_{sc}, below the melting line at T_{melt}. At T_{sc} the liquid spontaneously crystallizes, as the liquid becomes unstable with respect to the stable crystal. When the pressure is less than $P_{\text{sc,min}}$, the liquid becomes too glassy and we are no longer able to witness the crystallization. Interestingly, those versions of the model for which there is a LLCP present (those with a low f_q) crystallize more easily at lower pressures, suggesting a correlation between the existence of a LLCP and how easy it is for the liquid to crystallize.

of atoms within distance r, and thus we see in Fig. 3(a) that each atom has around 11.5 nearest neighbors in this crystal. This indicates a very compact structure; in fact, the highest number of nearest neighbors are in those crystals that have a face-centered cubic (fcc) or a hexagonal close-packed (hcp) crystal structure, both having 12 nearest neighbors for each atom.

To determine if the crystal is fcc-like or hcp-like, we consider in Fig. 3(b) the probability distribution of the Steinhardt/Lechner bond order parameter $\bar{q}_4$. In addition to a distribution obtained for our spontaneous crystal (thick black curve), we also plot the $\bar{q}_4$ distribution for a system with a perfect bcc crystal (blue), a perfect fcc crystal (red), and a perfect hcp crystal (green). Fig. 3(b) clearly indicates that the Si ions in the crystal have a fcc-like structure.

The fcc unit cell has two types of interstitial sites: 4 octahedral and 8 tetrahedral sites. If all the octahedral sites of the parent fcc lattice are filled by ions of the opposite charge, then the structure formed is the so-called rock-salt structure (the primary example being rock salt, NaCl). If instead all the tetrahedral sites of the parent fcc lattice are filled, then we attain the *fluorite structure*. This structure is named after calcium fluoride (CaF_2) which occurs in nature as the mineral fluorite. Since mWAC has a 1:2 ratio of Si and O ions (because it was derived from a model for silica, SiO_2), we may expect that mWAC crystallizes into a fluorite structure as well.

We therefore construct an elongated box with the Si and O ions placed according to the fluorite structure, and with the lattice vectors aligned in the x-, y-, and z-direction. Next, we

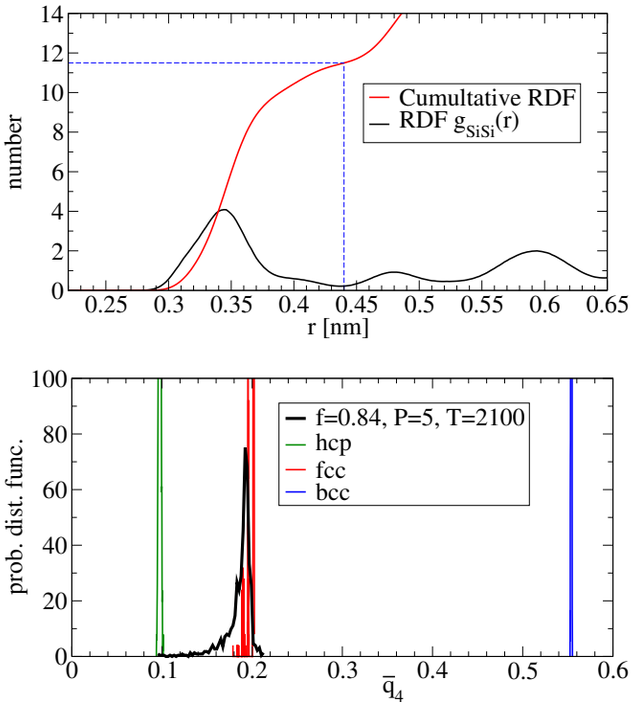

FIG. 3. **The crystal obtained through spontaneous nucleation has a fcc-like structure for $f_q = 0.84$ at 5 GPa, 2100 K.** (a) The Si-Si radial distribution function (RDF) and its integral the cumulative radial distribution function (CRDF) can be used to determine the average number of nearest Si neighbors around each Si ion. The nearest neighbors are those Si ions that lie within the first peak of the RDF, i.e., those with $r < 0.44$ nm. The CRDF indicates that, on average, there are about 11.5 Si ions within 0.44 nm, which means that this crystal has a coordination number of about 11-12. Note that the face-centered cubic (fcc) crystal and the hexagonal close-packed (hcp) crystal are known to have 12 nearest neighbors. (b) The histogram of the Steinhardt-Lechner parameter $\bar{q}_4$ closely matches that of a perfect fcc lattice (red), as opposed to bcc (blue) or hcp (green).

simulate the box with ions using the mWAC potential, initially at $T = 0$ and $P = 0$. We then carefully increase the temperature and pressure until we reach a point on the homogeneous nucleation line (e.g., 2100 K at 5 GPa for the case of $f_q = 0.84$). Visual inspection using a program such as VMD[89,90] is used to confirm that no crystal defects were created during this process. The resulting crystal structure for $f_q = 0.84$ is shown in Fig. 4(b), together with the fluorite structure it had initially in Fig. 4(a). The structure of the mWAC crystal produced via spontaneous crystallization, is found to have an orthorhombic lattice with sides approximately equal to $0.46 \times 0.49 \times 0.53$ nm. To confirm that we have created a defect-free version of the crystal that was obtained through spontaneous crystallization, we compare the Si-Si, Si-O, and O-O radial distribution functions of both our perfect crystal with those of the spontaneous crystal. Figs. 4(c)-(e) show an excellent overlap, thus indicating that we have indeed succeeded in finding the correct crystal structure.

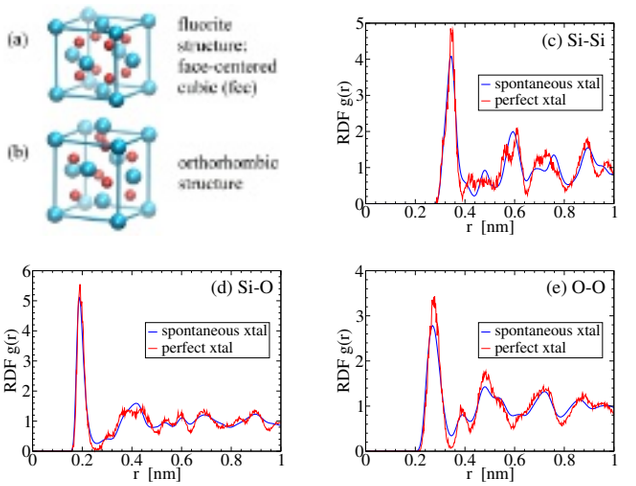

FIG. 4. **Confirmation that our "perfect" defect-free crystal matches the one obtained from spontaneous crystallization.** (a) The creation of a "perfect" defect-free crystal starts with manually constructing the fluorite structure, which is a common motif for compounds with the formula AB_2 (such as SiO_2). In the mWAC model, this crystal structure has the "Si" ions (blue) on a face-centered cubic (fcc) lattice with the "O" ions (red) located at the eight tetrahedral interstitial sites. (b) As we slowly raise the temperature to 2100 K and the pressure to 5 GPa (using the $f_q = 0.84$ model), we find that the fluorite structure changes into a base-centered orthorhombic crystal structure. (c)-(e) To confirm that the perfect orthorhombic crystal is identical to the crystal obtained from spontaneous crystallization, we calculate the radial distribution function (RDF) $g(r)$ for Si-Si, Si-O, and O-O. The RDFs of the spontaneous crystal are smoother because of defects and larger thermal fluctuations, but are otherwise identical to those of the perfect crystal.

C. Spontaneous melting and the melting line

In the same way one can supercool a liquid to a temperature below the melting line, one can also superheat a crystal to a temperature above the melting temperature[72–74]. A small disturbance in the crystal lattice—typically a crystalline defect—is needed to nucleate the melting process, although at sufficiently high temperatures the thermal fluctuations provide enough instability to initiate the melting. In the previous subsection we constructed a perfect crystal without any defects, which we can superheat to determine at what temperature $T_{\rm sm}$ it spontaneously melts. We simulate the crystal at different temperatures and pressures, and find that short runs of 1000 ps is sufficient to see the crystal remain solid or liquefy. It is easy to detect if the crystal has melted by looking at the potential energy $E_{\rm pot}$ and the density ρ. When a phase transition occurs, a sudden jump is clearly visible in either $E_{\rm pot}$ and/or ρ. Plotting these as a function of temperature allows us to determine at which temperature $T_{\rm sm}$ spontaneously melting occurs.

The melting line should lie somewhere in between the liquid spinodal (close to the homogeneous nucleation line) and the crystal spinodal (where the superheated crystal melts). At the melting temperature $T_{\rm m}$ the liquid is in a stable equilibrium with the crystal. Hence, we construct an elongated box of size

$2L \times L \times L$ that is half liquid and half crystal, and simulate it at different temperatures and pressures to determine at which $T > T_m$ the system completely melts and at which $T < T_m$ the whole box fully crystallizes. To create a simulation box that is half liquid / half crystal, we start with a box that is initially 100% crystal. We then add some random noise to the positions of the atoms that lie within $L/2 < x < 3L/2$, enough to locally destroy the crystal structure and turn that part of the crystal into a liquid. This box that is half liquid and half crystal is then simulated for about 1000 ps at constant pressure P and constant temperature T. If the box fully crystallizes then we know that T lies below T_m; if we find that crystal melts then we know that the temperature T lies above the melting temperature.

Although this method is rather crude (the simulations are often too short to allow the liquid to equilibrate) we find that it is sufficient to provide a decent estimate of the melting line, as demonstrated in Fig. 5. This figure shows the melting line for the $f_q = 0.84$ model with box sizes $N = 1536$, 3000, 5184, 8323, and 12288 ions. Since all curves with $N \geq 3000$ ions overlap, we conclude that with $N = 3000$ there are no significant finite-size effects. To obtain the data for Fig. 5, we start each simulation with a box that is 50% orthorhombic crystal and 50% liquid. We then run this system at different temperatures and constant pressure for 1000 ps to determine below which temperature T_{min} the system always fully crystallizes and above which temperature T_{max} the box always fully liquefies. The error bars in Fig. 5 indicate the range $[T_{min}, T_{max}]$ and thus illustrate the level of uncertainty in the melting temperature. The small error bars signify that 1000 ps is a sufficiently long run time to compensate for the slow evolution of the crystal-liquid interface and obtain a good estimate of the melting line.

In Fig 6 we consider the results of simulations done with $f_q = 0.84$ at pressure $P = 5$ GPa. How the potential energy $E_{pot}(T)$ and the density $\rho(T)$ change with temperature T depends on what process we simulate. Supercooling the liquid ultimately leads to spontaneous crystallization at 2100 K (blue curve), while a box that consists initially of half liquid/half crystal melts above 4000 K and crystallizes below it (green curve). The red curve indicates what happens when we heat up the perfect orthorhombic crystal of Fig. 4(b). Interestingly, this curve shows *two* jumps instead of one, indicating that we are dealing with three different phases, as opposed to just the liquid and one crystal. Because the lattice vectors of the initial crystal are in the x-, y-, and z-direction, the second crystal inherits the same alignment, making structural analysis of the crystal straightforward. We find that the Si ions in the second crystal have a *face-centered cubic* (fcc) structure with lattice constant 0.50 nm.

The average positions of the O ions is at the tetrahedral interstitial sites of the fcc lattice, and thus we conclude that this crystal has the fluorite structure, as shown in Fig. 4(a). However, visual inspection of the fcc crystal indicates that the O ions are rarely to be found at their interstitial sites, but tend to be scattered throughout the crystal in an almost liquid-like manner. This observation invites us to consider the diffusivity of the Si and O ions in the orthorhombic and fcc crystals, which is plotted in Fig. 7. The three separate phases are clearly visible. At high temperatures, both the Si and O ions display a large amount of diffusion in the liquid phase, while the diffusivity of both ion types is practically zero at low temperatures in the orthorhombic crystal phase. Remarkably, at temperatures between approximately 4660 K and 5100 K (when the crystal is in its fcc phase), the O ions display a significant amount of diffusion while the Si ions remain stuck in their fcc crystal lattice.

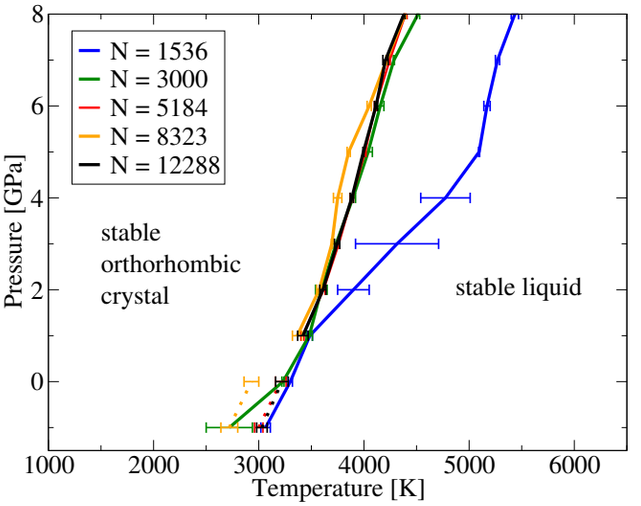

FIG. 5. **The melting line can be estimated using 1000 ps runs with 3000 ions.** Starting with a box of N ions that is 50% orthorhombic crystal and 50% liquid, we can estimate the melting temperature by running several 1000 ps simulations at constant pressure for different temperatures. Error bars with range $[T_{min}, T_{max}]$ indicate the temperature T_{min} at which the system always fully crystallizes and the temperature T_{max} above which the box always liquefies within 1000 ps. Dotted lines at low pressures and $N \geq 5184$ indicate runs for which we were unable to see the box completely crystallize; here T_{min} indicates the temperature below which the box always remains completely stuck in initial state of 50/50, while T_{max} still indicates the temperature above which the box always liquefies within 1000 ps. Overlap of all curves with $N \geq 3000$ ions indicates that $N = 3000$ is a sufficiently large box to prevent finite-size effects, and the small error bars indicate that 1000 ps is sufficiently long to obtain a decent estimate of the melting line.

Crystalline solids where one ion type can freely move while other ions are fixed in their crystal lattice are known as solid-state ionic conductors. An example of a similar material that displays this phenomenon is ceria (CeO_2), or Cerium(IV) oxide, which also forms a fluorite structure[91]. Because of their conductive properties, solid-state ionic conductors are of high interest for applications such as batteries, solid oxide fuel cells (SOFCs), and various sensors[92]. As water (H_2O) was the first liquid for which a LLCP was predicted, it must be noted that one of the many crystalline phases of ice also exhibits solid-state ionic conductivity. Around 100–400 GPa and 2000–3000 K, water forms ice XVIII, also known as superionic water or superionic ice[93]. This form of ice also has a face-centered cubic crystal structure.

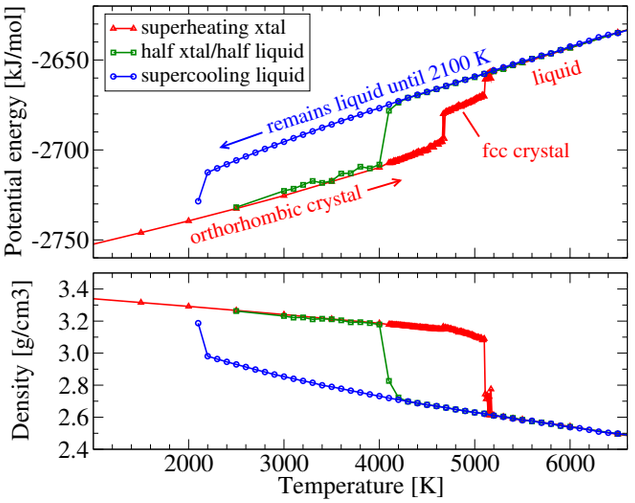

FIG. 6. **Determination of the liquid spinodal (blue), the crystal spinodal (red), and the melting line (green) for the $f_q = 0.84$ model at 5 GPa.** (a) Phase transitions are clearly visible when plotting the potential energy vs. the temperature. Blue curve: long simulations (up to 60 ns) of the liquid result in spontaneous crystallization at $T_{sc} = 2100$ K. Green curve: short simulations (1000 ps) that start as half liquid / half crystal, completely melt above 4000 K and completely crystallize below 4000 K, thus indicating that the crystal-liquid phase transition line is around 4000 K. Red curve: short simulations (1000 ps) of a box that consists initially of one large defect-free orthorhombic crystal behaves the same way as the 50% liquid / 50% simulations, except that the crystal remains intact at higher temperatures because a critical liquid nucleus must first occur before it melts. Near 4700 K the orthorhombic crystal does not liquefy, but instead transitions into a fcc (fluorite) structure. (b) The phase transitions are also visible as jumps in the density. However, the transition from orthorhombic to fcc crystal is not very clear, as both crystalline phases have almost the same density.

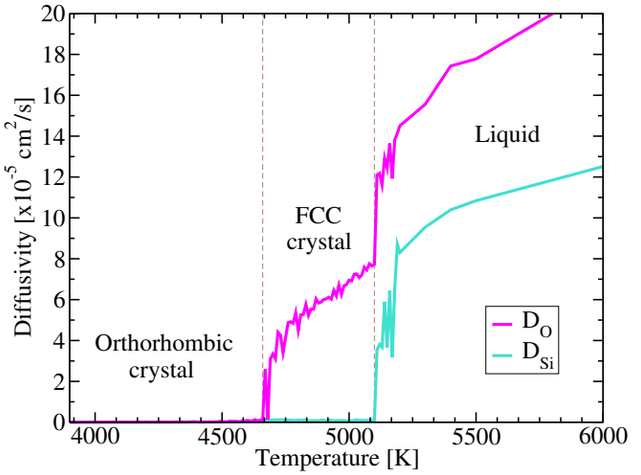

FIG. 7. **Solid-state ionic conductivity in the fcc crystalline phase of nonbonded mWAC model with $f_q = 0.84$.** Upon increasing the temperature of a defect-free orthorhombic crystal at $P = 5$ GPa, we observe a phase transition near 4660 K, where the orthorhombic lattice changes to a fcc lattice (the fluorite structure). Continued heating leads to the melting of this crystal into a liquid near 5100 K. Shown here are the diffusivity coefficients D_O of the O ions (magenta) and D_{Si} of the Si ions (turqoise). Both ion types show significant diffusion in the liquid ($T > 5100$ K), while diffusion is very limited for both ion types in the orthorhombic crystal ($T < 4660$ K). In the fcc crystal, however, the O diffusivity is liquid-like while the larger Si ions remain stuck in their lattice. This phenomenon is known as solid-state ionic conductivity and is known to occur in materials such as ceria (CeO_2)[91] and superionic ice[93].

D. Transitions in the phase diagrams

We follow the same procedure described in the previous subsections for $f_q = 0.72, f_q = 0.96$, and $f_q = 1.08$. The results are summarized in Fig. 8, which shows where all the transitions occur within the (T, P) phase diagram. Blue curves in Fig. 8 indicate a transition that happens upon cooling, while red curves represent transitions that occur upon heating. Green curves indicate that an elongated box with two different phases remains in that two-phase state even after running the simulation longer than 100 ns, thus indicating an equilibrium between those two phases. Solid lines indicate transitions between a crystal and the liquid, and dashed curves show the transitions between the two crystalline phases.

In Fig. 8 we consider all possible transitions between the three phases that were observed: the Orthorhombic (O) crystal phase, the FCC (F) crystal phase (which has a fluorite structure), and the Liquid (L). The red line labeled O→L, for example, indicates the transition from Orthorhombic to Liquid, which occurs upon heating. In addition to the transitions between those three phases, for $f_q = 0.96$ and 1.08 we also encounter a situation where a box that starts half liquid / half orthorhombic crystal remains in that state, even when cooled far below the melting temperature. In this situation crystallization is prevented by the slow kinetics of the liquid, i.e. the liquid has become a Glass (G). At high enough temperatures, the glass becomes sufficiently liquid that we witness the crystal melting. The lowest temperature at which we observe full liquefaction is indicated by the green dotted curve in Figs. 8(a) and (b), labeled G/O↔L.

Finally, we also include the results of several simulations done using a box that is 50% liquid and 50% beta-cristobalite crystal. Typically, in most models that have a LLPT, there is a crystal structure that is close in density and structure to the LDL state. In water, for example, the LDL phase is observed to form cubic ice, which is isostructural with beta-cristobalite in silica. However, the two crystal structures that we have found here are of a significantly higher density than both HDL and LDL. For instance, with $f_q = 0.84$ the density of both crystals is in the range 3.1–3.2 g/cm^3 while the liquid has a density of about 1.9–2.1 g/cm^3 for HDL and 1.5–1.6 g/cm^3 for LDL[58]. We therefore run several simulations with a box that is 50% liquid and 50% beta-cristobalite crystal, hoping to find a region in the phase diagram where the box starts to crystallize. Unfortunately, for all temperatures and pressures we considered, we were unable to observe the beta-cristobalite crystal growing. At temperatures above the orange dotted curves in

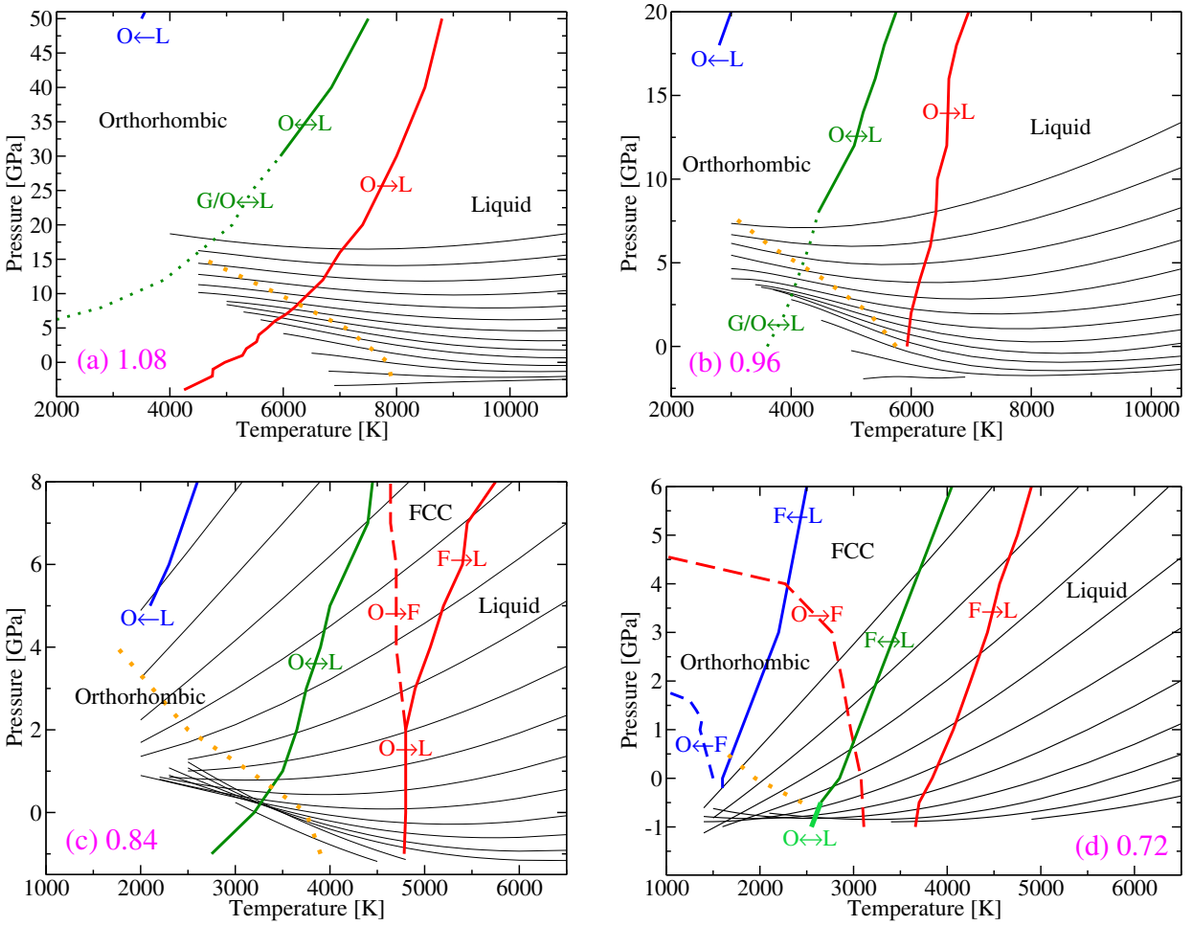

FIG. 8. **Phase transitions in the nonbonded mWAC model with (a) $f_q = 1.08$, (b) $f_q = 0.96$, (c) $f_q = 0.84$, and (d) $f_q = 0.72$.** Thin black curves are the same isochores as shown in Fig. 1. Clearly visible in panel (c) are the crossing isochores, which indicate that there is a LLCP in the $f_q = 0.84$ model. Blue curves highlight the transitions that happens upon supercooling the liquid, i.e., the spontaneous crystallization of the Liquid into the Orthorhombic crystal (O←L) and into the FCC crystal (F←L). Red curves show the transitions that occur upon superheating a crystal, i.e., the spontaneous melting of the Orthorhombic crystal to Liquid (O→L) and the FCC crystal to Liquid (F→L), as well as the transition from Orthorhombic to FCC crystal (dashed lines labeled O→F) Solid green curves indicate the melting line, where the crystal phase is in equilibrium with the liquid. For $f_q = 1.08$ and 0.96, we cannot identify the melting line at low pressures, as the liquid becomes too glassy; a box that is half crystal/half liquid would neither crystallize nor liquefy. The highest temperature at which the box still liquefies is indicated here with a dotted green curve labeled G/O↔L. Orange dotted lines represent simulations done with a box that is initially 50% liquid and 50% beta-cristobalite crystal. At temperatures above the orange dotted lines the box liquefies completely; at temperatures below these lines the box remains stuck in its initial state.

Fig. 8 the box with 50% liquid and 50% beta-cristobalite crystal is found to fully liquefy. At temperatures below this curve, the box remains stuck in its initial state because the liquid is too glassy to either liquefy or crystallize within the run times available to us.

There are several scenarios that can explain our observations. Firstly, it's possible that beta-cristobalite (or a similar structure) is indeed a stable phase at low temperatures and pressures, but we are unable to witness its crystallization because the kinetics is too slow. Alternatively, it is possible that in the modified-WAC model the meta-stable LDL crystallizes into a structure with a far higher density, unlike what has been observed for several models for water and silica. Future studies involving free energy calculations might help us answer this question.

Fig. 8 does show several interesting differences between the models without a LLCP ($f_q = 1.08, 0.96$) and those that do have a LLCP ($f_q = 0.84, 0.72$). For instance, with $f_q = 1.08$ we only observe the orthorhombic crystal structure, while we find both the orthorhombic and the fcc (fluorite) structure when $f_q = 0.72$ and 0.84. This supports the view that LLPTs typically occur in liquids that display polymorphism (the existence of multiple stable crystal structures).

Furthermore, we see that the glass/orthorhombic-crystal to liquid transition (G/O↔L) only occurs in the models that do not have a LLCP, and is much more pronounced for $f_q = 1.08$. In other words, for the nonbonded mWAC model, when there is no LLCP, the liquid becomes more glassy near the melting

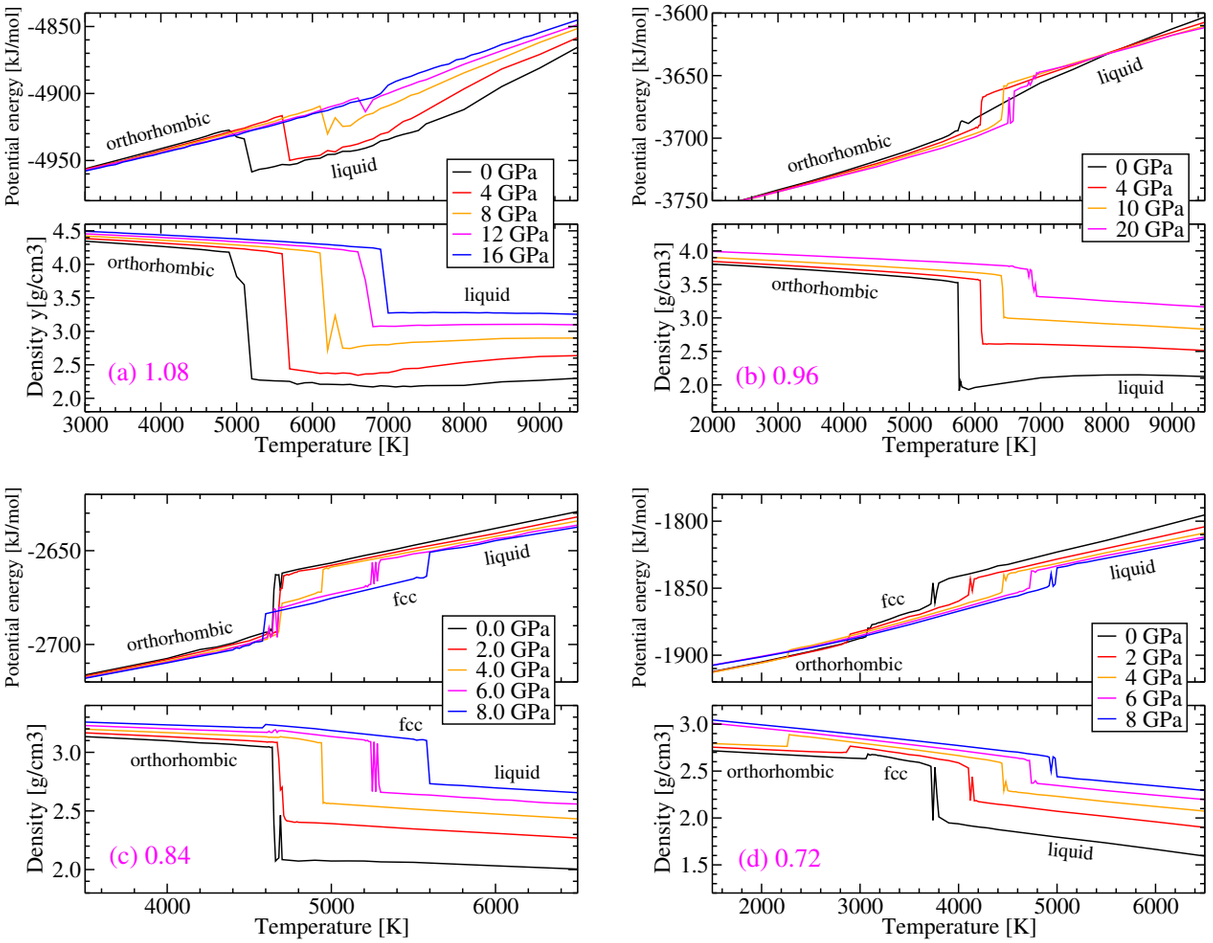

FIG. 9. **Jumps in potential energy and density at phase transitions when we superheat the orthorhombic crystal for (a) $f_q = 1.08$, (b) $f_q = 0.96$, (c) $f_q = 0.84$, and (d) $f_q = 0.72$.** Short simulations (1000 ps) of a superheated orthorhombic crystal at different temperatures produce clear transitions to either the fcc crystal or the liquid. In all cases the potential energy rises when the crystal transitions to a new phase, except for $f_q = 1.08$ as shown in panel (a). Transitions shown here correspond to the red curves shown in Fig. 8.

temperature. This observation goes hand-in-hand with the observation that the homogeneous nucleation line "disappears" to higher pressures for $f_q = 1.08$, as shown in Fig. 2. Those versions of the model that lack the LLCP seem to be relatively more glassy at low T and low P than those versions of the model that do have a LLCP. This supports, as noted by others[94], a possible relation between the location of the glass transition and the occurrence of a LLCP.

Finally, we must note that for $f_q = 0.84$ the melting line lies very close to the LLCP, making it difficult to tell for certain if the LLCP in this model is a critical point between two stable liquids or between two meta-stable liquids. We have a similar situation for $f_q = 0.72$, thus the question remains if the LLCP in mWAC is between two stable liquids.

Some interesting observations can also be made when we look at how $E_{\rm pot}(T)$ and $\rho(T)$ change as we adjust f_q. These results are shown in Fig. 9, for all four versions of the model considered. In all cases we start with the fluorite structure of Fig. 4(a) at very low temperatures. This crystal quickly transforms to either the orthorhombic or the fcc crystal, depending on the pressure and the value of f_q. We take this crystal and simulate it for 1000 ps at different temperatures and pressures. This short time is sufficient to obtain a decent estimate of any transitions; a phase transition shows itself as a sudden jump in the graph of $E_{\rm pot}(T)$ and/or $\rho(T)$, which are clearly visible in Fig. 9. All transitions observed this way are depicted in Fig. 8 as the red curves, since these transitions correspond to the temperatures close to the crystal spinodals. For example, in Fig. 9(a) there is a jump in both $E_{\rm pot}$ and ρ near 5000 K for $P = 0$ GPa, which corresponds to a point on the red O→L line at $(T, P) = (5000\ {\rm K}, 0\ {\rm GPa})$ in Fig. 8(a).

Of particular interest is how the potential energy $E_{\rm pot}(T)$ behaves differently for $f_q = 1.08$. In Fig. 9(a) we see that, upon heating, the potential energy suddenly *drops* when the orthorhombic crystal melts into the liquid. In comparison, when a crystal melts in Fig. 9(b), 9(c), and 9(d), there is instead a sudden *increase* in the potential energy. We must note, however, that these results are from 1000-ps simulations—

typically less time than what is required for the liquid to reach equilibrium. The E_{pot} and ρ are therefore not that of the liquid, but of a glass that forms immediately after the crystal has melted.

IV. CONCLUSIONS

As shown in earlier studies[57,58], adjusting the f_q parameter of the nonbonded modified-WAC (mWAC) model introduces a liquid-liquid critical point (LLCP). With $f_q = 1.08$ the model has no LLCP, but lowering this value to 0.84 introduces a LLCP which can be clearly identified from the crossing of the isochores in Fig. 1. As f_q is reduced further to 0.72, the LLCP disappears below the vapor line. Because of the close connection between the crystal phase and the LLCP[31,56,70], we expected significant changes regarding the crystalline phase as we reduce the f_q parameter from 1.08 to 0.72. The results in this work confirm that hypothesis.

By superheating a perfect (defect-free) crystal, we discovered the existence of a second crystalline phase for $f_q = 0.84$ and 0.72, i.e., those models that have a LLCP. This agrees with the observation that materials which exhibit a LLCP tend to have multiple allotropes, as mentioned in the Introduction. For the nonbonded modified-WAC model, the primary crystalline phase is an orthorhombic version of the fluorite structure, shown in Fig. 4(b). The second crystalline phase (clearly present when there is a LLCP) was found to have the Si ions positioned in a face-centered cubic (fcc) lattice with the smaller O ions near the eight tetrahedral interstitial sites, i.e., the fluorite structure of Fig. 4(a).

Interestingly, the O ions display liquid-like mobility inside the fcc crystal (see Fig. 7). This is a phenomenon known as solid-state ionic conduction, which is a material property used in batteries and fuel cells. It is unclear if there is any connection between this phenomenon and the LLCP, although it must be noted that ice XVIII (also known as superionic water or superionic ice) also exhibits solid-state ionic conduction[93], and that water is one of the many liquids for which a LLCP has been predicted.

In addition to finding multiple crystal structures, adjusting f_q also affects the propensity of crystallization. In particular, we find that spontaneous crystallization only happens at very high pressures for $f_q = 1.08$ while those models that do have a LLCP more readily crystallize (see Fig. 2). It is quite possible that the presence of a critical point leads to larger thermodynamic fluctuations in its vicinity, destabilizing the meta-stable liquid, causing it to crystallize more rapidly.

Possibly related to this is our inability to identify the melting line at low pressures for $f_q = 1.08$ and 0.96 (the green lines labeled O↔L in Fig. 8). At low temperatures and low pressures, the liquid becomes so slow and glassy that we are unable to witness any crystallization or melting of a box that is initially half liquid / half crystal. Instead, the box remains stuck in its initial state for at least hundreds of nanoseconds. On other hand, when the model has a LLCP, the liquid remains mobile enough to allow the formation of crystal nuclei in the liquid (or liquid nuclei in the crystal), making it possible to trace the melting line all the way down to negative pressures for $f_q = 0.84$ and 0.72.

For $f_q = 0.84$ we find that the melting line lies incredibly close to the LLCP. Our results suggest that the LLCP is located at slightly higher temperatures than the melting temperature, which would imply that the LLPT is between two *stable* liquids as opposed to a transition between two *meta-stable* liquids (meta-stable with respect to the orthorhombic crystal). Future studies providing a more detailed analysis of the melting line should establish if this is indeed the correct scenario.

Unusual behavior of the potential energy E_{pot} was observed regarding the phase transition from superheated orthorhombic crystal to liquid. When $f_q = 1.08$ we find in Fig. 9(a) that the potential energy goes *down* when the superheated crystal melts, while for $f_q = 0.96$, 0.84, and 0.72 the potential energy jumps *up* when we increase the temperature. The significance of this phenomenon as well as its connection with the LLCP remains unclear and will be studied in more detail in the future.

The results presented in this work form the first step to better understanding the behavior of the crystalline phase in the modified-WAC model, and with that the connections between the LLCP and the crystalline phase. There are many variables that we have not considered here, for instance the time scales involved regarding melting and freezing, how the diffusivity changes with f_q, etc. Furthermore, it is possible that the nonbonded modified WAC model discussed here has additional crystal phases that we have not observed yet. Similarly to having LLPTs between meta-stable liquids, it is quite possible that meta-stable crystals exist in this model, hidden behind the stable crystals that we do observe. Unfortunately, since we do not know the structure of these crystals, it is difficult to establish if these in fact exist or not. Finally, we hope to study the connection between crystallization and the LLCP in other versions of this model, not just the nonbonded version. Adjusting more model parameters should help determine which observations are model-specific and which are universal connections between the LLCP and the crystal phase.

AUTHOR DECLARATIONS

Conflict of Interest

The authors have no conflicts to disclose.

Author Contributions

E. Lascaris: Conceptualization; Data curation; Formal analysis; Funding acquisition; Investigation (equal); Methodology; Project Administration; Resources; Software (lead); Supervision; Validation (equal); Visualization (equal); Writing – original draft; Writing – review & editing (equal). **F. Marchese**: Investigation (equal); Software (supporting); Validation (equal); Visualization (equal); Writing – review & editing (equal). **N. Gaspar**: Investigation (equal); Software (sup-

porting); Validation (equal); Visualization (equal); Writing – review & editing (equal).

DATA AVAILABILITY

The data that support the findings of this study are available from the corresponding author (E. Lascaris) upon reasonable request.

REFERENCES

[1]P. H. Poole, T. Grande, C. A. Angell, and P. F. McMillan, *Science* **275**, 322 (1997).
[2]P. H. Poole, F. Sciortino, U. Essmann, and H. E. Stanley, *Nature* **360**, 324 (1992).
[3]F. H. Stillinger and A. Rahman, *J. Chem. Phys.* **60**, 1545 (1974).
[4]P. H. Poole, F. Sciortino, U. Essmann, and H. E. Stanley, *Phys. Rev. E* **48**, 3799 (1993).
[5]P. H. Poole, U. Essmann, F. Sciortino, and H. E. Stanley, *Phys. Rev. E* **48**, 4605 (1993).
[6]F. Sciortino, P. H. Poole, U. Essmann, and H. E. Stanley, *Phys. Rev. E* **55**, 727 (1997).
[7]P. Gallo, K. Amann-Winkel, C. A. Angell, M. A. Anisimov, F. Caupin, C. Chakravarty, E. Lascaris, T. Loerting, A. Z. Panagiotopoulos, J. Russo, J. A. Sellberg, and H. E. Stanley, *Chem. Rev.* **116**, 7463 (2016).
[8]J. C. Palmer, P. H. Poole, F. Sciortino, and P. G. Debenedetti, *Chem. Rev.* **118**, 9129 (2018).
[9]D. T. Limmer and D. Chandler, *J. Chem. Phys.* **135**, 134503 (2011).
[10]Y. Liu, J. C. Palmer, A. Z. Panagiotopoulos, and P. G. Debenedetti, *J. Chem. Phys.* **137**, 214505 (2012).
[11]J. C. Palmer, R. Car, and P. G. Debenedetti, *Faraday Discuss.* **167**, 77 (2013).
[12]D. T. Limmer and D. Chandler, *J. Chem. Phys.* **138**, 214504 (2013).
[13]T. A. Kesselring, E. Lascaris, G. Franzese, S. V. Buldyrev, H. J. Herrmann, and H. E. Stanley, *J. Chem. Phys.* **138**, 244506 (2013).
[14]P. H. Poole, R. K. Bowles, I. Saika-Voivod, and F. Sciortino, *J. Chem. Phys.* **138**, 034505 (2013).
[15]J. C. Palmer, F. Martelli, Y. Liu, R. Car, A. Z. Panagiotopoulos, and P. G. Debenedetti, *Nature* **510**, 385 (2014).
[16]V. Holten, J. C. Palmer, P. H. Poole, P. G. Debenedetti, and M. A. Anisimov, *J. Chem. Phys.* **140**, 104502 (2014).
[17]F. Smallenburg, P. H. Poole, and F. Sciortino, *Mol. Phys.* **113**, 2791 (2015).
[18]D. Hohl and R. O. Jones, *Phys. Rev. B* **50**, 17047 (1994).
[19]Y. Katayama, T. Mizutani, W. Utsumi, O. Shimomura, M. Yamakata, and K.-I. Funakoshi, *Nature* **403**, 170 (2000).
[20]Y. Katayama, *J. Non-Cryst. Solids* **312**, 8 (2002).
[21]Y. Katayama, Y. Inamura, T. Mizutani, M. Yamakata, W. Utsumi, and O. Shimomura, *Science* **306**, 848 (2004).
[22]L. M. Ghiringhelli and E. J. Meijer, *J. Chem. Phys.* **122**, 184510 (2005).
[23]L. M. Ghiringhelli and E. J. Meijer, *J. Phys.: Condens. Matter* **19(41)**, 416104 (2007).
[24]L. I. Aptekar, *Sov. Phys. Dokl.* **24**, 993 (1979).
[25]S. Sastry and C. A. Angell, *Nature Mater.* **2**, 739 (2003).
[26]V. V. Vasisht, S. Saw, and S. Sastry, *Nature Phys.* **7**, 549 (2011).
[27]N. Jakse and A. Pasturel, *Phys. Rev. Lett.* **99**, 205702 (2007).
[28]P. Ganesh and M. Widom, *Phys. Rev. Lett.* **102**, 075701 (2009).
[29]M. Beye, F. Sorgenfrei, W. F. Schlotter, W. Wurth, and A. Föhlisch, *Proc. Natl. Acad. Sci. U.S.A.* **107**, 16772 (2010).
[30]R. Winter, P. A. Egelstaff, W.-C. Pilgrim, and W. S. Howells, *J. Phys.: Condens. Matter* .
[31]L. Henry, M. Mezouar, G. Garbarino, D. Sifré, G. Weck, and F. Datchi, *Nature* **584**, 382 (2020).
[32]J. N. Glosli and F. H. Ree, *Phys. Rev. Lett.* **82**, 4659 (1999).
[33]M. Togaya, *Phys. Rev. Lett.* **79**, 2474 (1997).
[34]P. H. Poole, M. Hemmati, and C. A. Angell, *Phys. Rev. Lett.* **79**, 2281 (1997).
[35]I. Saika-Voivod, F. Sciortino, and P. H. Poole, *Phys. Rev. E* **63**, 011202 (2000).
[36]C. A. Angell and M. Hemmati, Glass Transitions and Critical Points in Orientationally Disordered Crystals and Structural Glassformers: "Strong" Liquids are More Interesting Than We Thought, in *4th International Symposium on Slow Dynamics in Complex Systems*, edited by M. Tokuyama and I. Oppenheim, volume 1518, p. 9, AIP Conf. Proc., 2013.
[37]E. Lascaris, M. Hemmati, S. V. Buldyrev, H. E. Stanley, and C. A. Angell, *J. Chem. Phys.* **140**, 224502 (2014).
[38]J. Senker and E. Rössler, *Chem. Geol.* **174**, 143 (2001).
[39]H. Tanaka, R. Kurita, and H. Mataki, *Phys. Rev. Lett.* **92**, 025701 (2004).
[40]R. Kurita and H. Tanaka, *Science* **306**, 845 (2004).
[41]R. Shimizu, M. Kobayashi, and H. Tanaka, *Phys. Rev. Lett.* **112**, 125702 (2014).
[42]M. Kobayashi, R. Shimizu, and H. Tanaka, *J Phys Chem B.* **119(35)**, 11768 (2015).
[43]K.-I. Murata and H. Tanaka, *Proc. Natl. Acad. Sci. U.S.A.* **112**, 5956 (2015).
[44]M. Kobayashi and H. Tanaka, *Nat. Commun.* **7**, 13438 (2016).
[45]F. Walton, J. Bolling, A. Farrell, J. MacEwen, C. D. Syme, M. G. Jiménez, H. M. Senn, C. Wilson, G. Cinque, and K. Wynne, *J. Am. Ceram. Soc.* **142, 16**, 7591 (2020).
[46]Y. He, H. Li, Y. Jiang, X. Li, and X. Bian, *Sci. Rep.* **4**, 3635 (2014).
[47]I. Cohen, A. Ha, X. Zhao, M. Lee, T. Fischer, M. J. Strouse, and D. Kivelson, *J. Phys. Chem.* **100**, 8518 (1996).
[48]G. P. Johari and C. Ferrari, *J. Phys. Chem. B* **101**, 10191 (1997).
[49]C. Alba-Simionesco and G. Tarjus, *EPL* **52**, 297 (2000).
[50]B. G. Demirjian, G. Dosseh, A. Chauty, M.-L. Ferrer, D. Morineau, C. Lawrence, K. Takeda, D. Kivelson, and S. Brown, *J. Phys. Chem. B* **105**.
[51]G. Tarjus, C. Alba-Simionesco, M. Grousson, P. Viot, and D. Kivelson, *J. Phys.: Condens. Matter* **15**, S1077 (2003).
[52]A. Hédoux, Y. Guinet, P. Derollez, O. Hernandez, R. Lefort, and M. Descamps, *Phys. Chem. Chem. Phys.* **6**, 3192 (2004).
[53]A. Hédoux, Y. Guinet, P. Derollez, O. Hernandez, L. Paccou, and M. Descamps, *J. Non-Cryst. Solids* **352**, 4994 (2006).
[54]J. Baran, N. A. Davydova, and M. Drozd, *J. Chem. Phys.* **140**, 104512 (2014).
[55]M. Tarnacka, O. Madejczyk, M. Dulski, P. Maksym, K. Kaminski, and M. Paluch, *J. Phys. Chem. C* **121**, 19442 (2017).
[56]F. Smallenburg and F. Sciortino, *Phys. Rev. Lett.* **115**, 015701 (2015).
[57]E. Lascaris, *Phys. Rev. Lett.* **116**, 125701 (2016).
[58]R. Chen, E. Lascaris, and J. C. Palmer, *J. Chem. Phys.* **146**, 234503 (2017).
[59]J. Guo and J. C. Palmer, *Phys. Chem. Chem. Phys.* **20**, 25195 (2018).
[60]E. Lascaris, *J. Chem. Phys.* **157**, 204501 (2022).
[61]L. V. Woodcock, C. A. Angell, and P. Cheeseman, *J. Chem. Phys.* **65**, 1565 (1976).
[62]D. R. Peck, Phosphorus, in *Mellor's Comprehensive Treatise on Inorganic and Theoretical Chemistry*, volume VIII Supp. III, pp. 149–227, Longman, London, 1971.
[63]J. Donohue, *The Structure of the Elements*, Wiley & Sons, New York, 1974.
[64]M. Beekman, K. Wei, and G. S. Nolas, *Appl. Phys. Rev.* **3**, 040804 (2016).
[65]R. H. Wentorf, Jr and J. S. Kasper, *Science* **139**, 338 (1963).
[66]S. J. Duclos, Y. K. Vohra, and A. L. Ruoff, *Phys. Rev. B* **41**, 12021 (1990).
[67]M. I. McMahon and R. J. Nelmes, *Phys. Rev. B* **47**, 8337(R) (1993).
[68]B. D. Malone, J. D. Sau, and M. L. Cohen, *Phys. Rev. B* **78**, 035210 (2008).
[69]B. D. Malone, J. D. Sau, and M. L. Cohen, *Phys. Rev. B* **78**,

161202(R) (2008).
[70] H. Tanaka, *J. Chem. Phys.* **153**, 130901 (2020).
[71] P. G. Debenedetti, V. S. Raghavan, and S. S. Borick, *J. Phys. Chem.* **95**, 4540 (1991).
[72] M. Iwamatsu, *J. Phys.: Condens. Matter* **11**, L1 (1999).
[73] M. Forsblom and G. Grimvall, *Nature Mater.* **4**, 388 (2005).
[74] Q. S. Mei and K. Lu, **52**, 1175 (2007).
[75] F. Jensen, *Introduction to Computational Chemistry*, John Wiley & Sons, 2nd edition, 2007.
[76] M. Hemmati and C. A. Angell, *J. Non-Cryst. Solids* **217**, 236 (1997).
[77] H. Bekker, H. Berendsen, E. Dijkstra, S. Achterop, R. van Drunen, D. van der Spoel, A. Sijbers, H. Keegstra, and M. K. R. Renardus, Gromacs - A parallel computer for molecular dynamics simulations, in *Physics computing '92*, edited by R. A. DeGroot and J. Nadrchal, pp. 252–256, World Scientific, Singapore, 1993, 4th International Conference on Computational Physics (PC 92) ; Conference date: 24-08-1992 Through 28-08-1992.
[78] H. J. C. Berendsen, D. van der Spoel, and R. van Drunen, *Comp. Phys. Comm.* **91**, 43 (1995).
[79] E. Lindahl, B. Hess, and D. van der Spoel, *J. Mol. Mod.* **7**, 306 (2001).
[80] D. van der Spoel, E. Lindahl, B. Hess, G. Groenhof, A. Mark, and H. Berendsen, *J. Comp. Chem.* **26**, 1701 (2005).
[81] B. Hess, C. Kutzner, D. van der Spoel, and E. Lindahl, *J. Chem. Theory Comp.* **4**, 435 (2008).
[82] S. Pronk, S. Páll, R. Schulz, P. Larsson, P. Bjelkmar, R. Apostolov, M. R. Shirts, J. C. Smith, P. M. Kasson, D. van der Spoel, B. Hess, and E. Lindahl, *Bioinformatics* **29**, 845 (2013).
[83] J. D. Honeycutt and H. C. Andersen, *J. Phys. Chem.* **91**, 4950 (1987).
[84] C. L. Kelchner, S. J. Plimpton, and J. C. Hamilton, *Phys. Rev. B* **58**, 11085 (1998).
[85] A. Stukowski, *Model. Simul. Mater. Sci. Eng.* **20**, 045021 (2012).
[86] P. J. Steinhardt, D. R. Nelson, and M. Ronchetti, *Phys. Rev. B* **28**, 784 (1983).
[87] P. R. ten Wolde, M. J. Ruiz-Montero, and D. Frenkel, *J. Chem. Phys.* **104**, 9932 (1996).
[88] W. Lechner and C. Dellago, *J. Chem. Phys.* **129**, 114707 (2008).
[89] W. Humphrey, A. Dalke, and K. Schulten, *Journal of Molecular Graphics* **14**, 33 (1996).
[90] J. Stone, An Efficient Library for Parallel Ray Tracing and Animation, Master's thesis, Computer Science Department, University of Missouri-Rolla, 1998.
[91] M. Brigante and P. C. Schulz, *Chem. Eng. J.* **191**, 563 (2012).
[92] S. Swaroop, M. Kilo, A. E. Kossoy, I. Lubomirsky, and I. Riess, *Solid State Ion.* **179**, 1205 (2008).
[93] M. Millot, F. Coppari, J. R. Rygg, A. Correa Barrios, S. Hamel, D. C. Swift, and J. H. Eggert, *Nature* **569**, 251 (2019).
[94] N. Giovambattista, T. Loerting, B. R. Lukanov, and F. W. Starr, *Sci. Rep.* **2**, 390 (2012).